Inorg. Chem. **2008**, *47*, 7651−7659

Approximant Phases and an Icosahedral Quasicrystal in the Ca−Au−Ga System: The Influence of Size of Gallium versus Indium

Qisheng Lin and John D. Corbett*

Department of Chemistry, Iowa State University, Ames, Iowa 50010

Received April 17, 2008

Two crystalline approximants (ACs) and their corresponding icosahedral quasicrystal (i-QC) are obtained in the Ca−Au−Ga system through conventional solid-state exploratory syntheses. Single crystal structural analyses reveal that the 1/1 AC, $Ca_3Au_xGa_{19-x}$ ($x = \sim 9.3-12.1$) [$Im\bar{3}$, $a = 14.6941(6)-14.7594(6)$ Å], has the empty cubes in the prototypic YCd_6 ($= Y_3Cd_{18}$) now fully occupied by Ga, resulting in a 3:19 stoichiometry. In parallel, the distorted cubes in the 2/1 AC, $Ca_{13}Au_{57.1}Ga_{23.4}$ [$Pa\bar{3}$, $a = 23.9377(8)$ Å] are fully or fractionally occupied by Ga. The valence electron count per atom (e/a) for the 2/1 AC (1.64) is smaller than that over the 1/1 AC composition range (1.76−2.02), and the e/a of the $Ca_{15.2}Au_{50.3}Ga_{34.5}$ i-QC, 1.84, is somewhat distant from typical values for Tsai-type i-QCs ($\sim$ 2.0). Comparisons of the gallium results with the corresponding In phases suggest that the structural differences result mainly from size rather than electronic factors. The 1/1 and 2/1 appear to be thermodynamically stable on slow cooling, as usual, whereas the i-QC isolated by quenching decomposes on heating at $\sim$660 °C, mainly into 2/1 AC and $Ca_3(Au,Ga)_{11}$. Calculations of the electronic structure of 1/1 AC suggest that the Fermi sphere−Brillouin zone interactions remain important for the Ca−Au−Ga i-QC.

Introduction

The discovery of the first icosahedral quasicrystal (i-QC) in an Al−Mn alloy[1] broke a serenity within the realm of traditional crystallography because this material exhibited a non-crystallographic icosahedral symmetry.[2] Later on, scientists from diverse fields intensively baked QCs with respect to different aspects (theory, synthesis, structure, properties, etc.), possibly driven by the experience (or lesson) that a new type of material might have unpredicted applications, as nanoscale materials have in recent years. Actually, QCs play unique roles in the understanding of some basic theories (e.g., friction on surfaces[3]) and of high dimensional crystallography. However, two decades have passed and the major applications of QCs and their crystalline neighbors, approximants,[4] remain limited to specific alloys and to surface coating materials, despite evidence that some QCs appear to posses potential merit as thermoelectrics,[5] catalysts,[6] and hydrogen storage,[7] photonic,[8,9] and bio materials.[10] The reasons may have substantial connections with the small number of known QCs. After all, there are to date no more than 200 QC systems, and only about one-third of them are thermodynamically stable ones.[11] This fact suggests that development of novel QC/AC systems remains the bedrock of further studies of QCs.

Not many chemists are well informed about QC/ACs though. One starting place are Hume−Rothery mechanisms,[12] which are also considered to play important roles in the electronic stabilization of many QCs.[13] To chemists, therefore, knowledge about the interplay among composition, crystal structure, electronic structure, and properties acquired

* To whom correspondence should be addressed. E-mail: jcorbett@iastate.edu.

(1) Shechtman, D.; Blech, I.; Gratias, D.; Cahn, J. W. *Phys. Rev. Lett.* **1984**, *53*, 1951.
(2) Janot, C. *Quasicrystals: A Primer*, 2nd ed.; Oxford University Press: Oxford, U.K., 1994.
(3) Park, J. Y.; Ogletree, D. F.; Salmeron, M.; Ribeiro, R. A.; Canfield, P. C.; Jenks, C. J.; Thiel, P. A. *Science* **2005**, *309*, 1354.
(4) Goldman, A. I.; Kelton, K. F. *Rev.Mod. Phys.* **1993**, *65*, 213.
(5) Macia, E. *Appl. Phys. Lett.* **2000**, *77*, 3045.
(6) Kameoka, S.; Tanabe, T.; Tsai, A. P. *Catal. Today* **2004**, *93*−*95*, 23.
(7) Kelton, K. F.; Gibbons, P. C. *MRS.Bull.* **1997**, *22*, 71.
(8) Freedman, B.; Bartal, G.; Segev, M.; Lifshitz, R.; Christodoulides, D. N.; Fleischer, J. W. *Nature* **2006**, *446*, 1166.
(9) Freedman, B.; Lifshitz, R.; Fleischer, J. W.; Segev, M. *Nat. Mater.* **2007**, *6*, 776.
(10) Andersen, B. C.; Bloom, P. D.; Baikerikar, K. G.; Sheares, V. V.; Mallapragada, S. K. *Biomaterials* **2002**, *23*, (1761)
(11) Steurer, W.; Deloudi, S. *Acta Crystallogr.* **2008**, *A64*, 1.
(12) Hume-Rothery, W. *J. Inst. Met.* **1926**, *35*, 295.
(13) Mizutani, U. In *The Science of Complex Alloy Phases*; Massalski, T. B., Turchi, P. E. A., Eds.; TMS (The Minerals, Metals & Materials Society): Warrendale, PA, 2005; pp 1−42.

10.1021/ic800694j CCC: $40.75
Published on Web 08/02/2008

in the study of polar intermetallic and Zintl phases may greatly aid explorations for novel QCs/ACs. For example, the polar alkali-metal intermetallics containing heavier triels (Ga, In, Tl) exhibit distinctive structural regularities: thallium examples in general exhibit isolated empty or filled icosahedra, whereas Ga- and In-rich intermetallic phases feature more extended frameworks of condensed icosahedra and related clusters.[14–17] Clusters with icosahedral symmetry are commonly accepted as the building blocks of QC/ACs. Therefore, we speculate that selected polar intermetallic or Zintl phases containing triel elements (particularly for, but not limited to, Ga and In) might, under optimal conditions, be structurally and electronically tuned to ACs and, eventually, to QCs.[18] In addition, late transition metals as third components can be good "electron buffers" in tuning to QC/AC phases; they generally reduce the overall valence electron counts per atom (*e/a*), thus affording opportunities to push *e/a* closer to or into the region of Hume−Rothery phases (<2.0).

The forementioned understandings have been particularly applicable to the Tsai-type icosahedral QCs (i-QCs),[19] for which the 1/1 ACs are isostructural with the prototypic YCd_6.[20] For example, the $ScZn_6$ phase,[21] earlier mis-reported as Sc_3Zn_{17},[22] can be gradually converted into AC and QC phases as *y* in the $Sc_3Cu_yZn_{18-y}$ formula is increased from 0 to ∼2.2.[21,23] The discoveries of other i-QCs in Sc−M−Zn (M = Ni, Fe, Co) systems by other groups also appear to follow similar intuition or experience.[24] Other examples[18,25–29] include the utilization of electronic tunings to gain the ACs and i-QCs from the isotypic $Mg_2Cu_6Ga_5$, Mg_2Zn_{11}, and $Na_2Au_6In_5$. On one hand, these Mg_2Zn_{11}-type compounds can be viewed in terms of simple cubic packing of endohedral clusters containing, successively from the center out, an icosahedron, a pentagonal dodecahedron, and a larger icosahedron, all with local icosahedral symmetries. On the other hand, they have evidently similar-sized Fermi spheres and Brillouin zone boundaries, characteristic qualifications for the Hume−Rothery rules.

Our recent study of the Ca−Au−In system reveals that the $Ca_3Au_{12.2}In_{6.3}$ 1/1 AC and the $Ca_{12.6}Au_{37.0}In_{39.6}$ 2/1 AC exhibit considerable differences in shell contents and many more split positional disorder than the corresponding Sc−Mg−Zn ACs.[28,29] The disorder has nothing to do with the thermal history of samples, but it is possibly a result of a lower differentiation both radially (in size) and chemically between gold and indium elements. In this work, we report the syntheses, phase widths, and crystal structures of 1/1 and 2/1 ACs in the neighboring Ca−Au−Ga system, together with the evidence for the i-QC phase. We have also recently obtained the corresponding 1/0 AC, $CaAu_{3+x}Ga_{1-x}$ (x = 0−0.13).[30] The replacement of indium by the smaller gallium certainly provides an ideal playground for the study of size effects on crystal structures because in many cases indium and gallium have similar electronic contributions in polar intermetallics, and their difference in Mulliken electronegativities is minimal; Ga, 3.2 eV; In, 3.1 eV.[31]

Experimental Section

Syntheses. Elements as calcium chunks, gallium ingots, and gold sheets (all >99.99%, Alfa-Aesar) were weighed (±0.1 mg) in a N_2-filled glovebox with moisture levels below 0.1 ppmv. The mixtures (∼400 mg) were placed in tantalum containers that were then weld-sealed under an argon atmosphere and in turn enclosed within evacuated SiO_2 jackets (>10^{-6} torr). Samples were typically treated with the following reaction temperature profile: heat to 850 °C, hold at this temperature for 24 h, cool to 500 °C at a rate of 2 °C/h, and anneal there for three weeks. In contrast, samples of quasicrystals were obtained directly by quenching the containers at 850 °C into cold water, crushing the SiO_2 jacket immediately thereafter. All products are metallic, brittle, and relatively inert to moisture and air at room temperature. Selected reactions and products are given in Table 1, together with the lattice parameters for 1/1 and 2/1 ACs refined from powder data.

Thermal Analyses. 1/1, 2/1 ACs and *i*-QC samples (20−50 mg) were held in alumina crucibles which were mounted on the sample holder of a PerkinElmer Differential Thermal Analyzer (DTA-7). Samples were typically heated under Ar to 620 °C at a rate of 10 °C/min, kept at this temperature for 10 min, and cooled to 200 °C at the same rate. XRD patterns pre- and post-DTA scanning were also recorded for phase identification.

SEM-EDX. Elemental compositions were determined via semiquantitative energy-dispersive X-ray spectroscopy (EDX) on a JEOL 840A scanning electron microscope (SEM) with IXRF X-ray analyzer system and Kevex Quantum light-element detector. To avoid the influences of sample tilting, all samples (mounted in epoxy) were carefully polished. Samples were first scanned by means of back scattered electrons, through which different phases were represented by regions with different darknesses. Elemental proportions for selected single-phase areas were then measured. At least four readings were made (on different areas) for each interesting single-phase region, and the averages were used to compare with the compositions refined from single crystal X-ray diffraction data.

X-ray Diffraction. Phase identities and purities were checked on the basis of powder diffraction data collected on a Huber 670 Guinier powder camera equipped with an area detector and Cu $K\alpha_1$ radiation (λ = 1.540598 Å) and calibrated with LaB_6. The detection limit of a second phase with this instrument and system is conservatively estimated to be about 5 vol % in equivalent scattering

(14) Belin, C.; Tillard-Charbonnel, M. *Prog. Solid State Chem.* **1993**, *22*, 59.
(15) Corbett, J. D. In *Chemistry, Structure, and Bonding of Zintl Phases and Ions*; Kauzlarich, S. M., Ed.; VCH: New York, 1996; p 139.
(16) Corbett, J. D. *Angew. Chem., Int. Ed.* **2000**, *39*, 670.
(17) Miller, G. J.; Lee, C.-S.; Choe, W. In *Inorganic Chemistry Highlights*; Meyer, G., Naumann, D.; Wesemann, L., Eds.; Wiley-VCH: Weinheim, Germany, 2002; pp 21 −53.
(18) Lin, Q.; Corbett, J. D. *Inorg. Chem.* **2003**, *42*, 8762.
(19) Tsai, A. P.; Guo, J. Q.; Abe, E.; Takakura, H.; Sato, T. J. *Nature* **2000**, *408*, 537.
(20) Larson, A. C.; Cromer, D. T. *Acta Crystallogr.* **1971**, *27B*, 1875.
(21) Lin, Q.; Corbett, J. D. *Inorg. Chem.* **2004**, *43*, 1912.
(22) Andrusyak, R. I.; Kotur, B. Y.; Zavodnik, V. E. *Sov.Phys. Crystallogr.* **1989**, *34*, 600.
(23) Lin, Q.; Corbett, J. D. *Philos. Mag. Lett.* **2003**, *83*, 755.
(24) Ishimasa, T. In *The Science of Complex Alloy Phases*; Massalski, T. T., Turchi, P. E. A., Eds.; TMS (The Mineral, Metals & Materials Society): Warrendale, PA, 2005; p 231.
(25) Lin, Q.; Corbett, J. D. *Inorg. Chem.* **2005**, *44*, 512.
(26) Lin, Q.; Corbett, J. D. *J. Am. Chem. Soc.* **2005**, *127*, 12786.
(27) Lin, Q.; Corbett, J. D. *Philos. Mag.* **2006**, *86*, 607.
(28) Lin, Q.; Corbett, J. D. *J. Am. Chem. Soc.* **2006**, *128*, 13268.
(29) Lin, Q.; Corbett, J. D. *J. Am. Chem. Soc.* **2007**, *129*, 6789.
(30) Lin, Q.; Corbett, J. D. *Inorg. Chem.* **2008**, *47*, 3462.
(31) Pearson, R. G. *Inorg. Chem.* **1988**, *27*, 734.

Table 1. Loaded Reactions, Products at 500°C, and Refined Lattice Parameters (Å) for 1/1 and 2/1 ACs[a]

normalized Ca/Au/Ga (%)	*e/a*	products[b]	latt. para.[c]	remarks
10.0/30.0/60.0	2.30	15% 1/1 AC + 10% $Ca(Au,Ga)_4$ + 75% U_1	14.7042(6)	
10.0/40.0/50.0	2.10	65% 1/1 AC + 35% U_1	14.7145(6)	
10.0/50.0/40.0	1.90	95% 1/1 AC + U_2	14.7594(6)	crystal **3**
10.0/55.0/35.0	1.80	70% 1/1 AC + 30% 2/1 AC	14.790(1) 23.953(1)	
10.0/60.0/30.0	1.70	95% 2/1 AC + U_3	23.981(1)	
10.0/70.0/20.0	1.50	30% 2/1 AC + 65% 1/0 AC + U_3	23.9816(9)	
14.3/28.6/57.1	2.29	10% 1/1 AC + 60% $Ca(Au,Ga)_4$ + 30% U_1	14.6732(7)	
14.3/35.7/50.0	2.14	35% 1/1 AC + 50% $Ca(Au,Ga)_4$ + 15% U_1	14.6737(6)	
14.3/42.9/42.9	2.00	75% 1/1 AC + 25% $Ca_3(Au,Ga)_{11}$	14.6960(6)	
14.3/42.9/42.9	2.00	>95% 1/1 AC (by centrifuging)	14.6941(6)	crystal **1**
14.3/46.4/39.3	1.93	80% 1/1 AC + 20% $Ca_3(Au,Ga)_{11}$	14.7226(6)	
14.3/50.0/35.7	1.86	>95% 1/1 AC	14.7306(6)	crystal **2**
14.3/57.1/28.6	1.72	>95% 2/1 AC	23.9377(8)	crystal **4**
14.3/64.3/21.4	1.57	90% 2/1 AC + U_3	23.9620(8)	
15.0/52.5/32.5	1.80	80% 2/1 AC + 10% 1/1 AC + 10% $Ca_3(Au,Ga)_{11}$	23.8829(9)	
15.0/60.0/25.0	1.65	70% 2/1 AC + 30% 1/0 AC	23.9433(8)	

[a] All products were obtained by slowly cooling from melt and annealing at 500 °C for 3 weeks, except that crystal **1** was isolated by melt spinning method (see text). The i-QC is not observed at this temperature. [b] $Ca_3(Au,Ga)_{11}$ refers to solid solutions with same structure as $Ca_3Au_{6.6}Ga_{4.4}$,[42] whereas $Ca(Au,Ga)_4$, refers to solid solutions with same structure as $CaAu_{0.5}Ga_{3.5}$.[43] U_x denotes unidentified phases. [c] Lattice parameters were refined from five to nine of the strongest peaks within 20°−70° for 1/1 or 2/1 ACs, or for both if peaks were discernible.

power, so that an apparently single phase pattern is concluded to represent $a > 95\%$ phase purity. Peak searching was done with the aid of Winplotr,[32] and lattice parameter refinements were performed using program UnitCell.[33] The lattice parameters refined from powder data were used with single crystal refinements for bond distance calculations.

Single crystals were mounted on a Bruker APEX CCD single crystal diffractometer equipped with graphite-monochromatized Mo Kα ($\lambda = 0.71069$ Å) radiation. Room temperature intensity data were collected in a ω scan, within $2\theta = \sim 3-57°$, from 1315 frames defined by a hemisphere, with an exposure of 30 s/frame. Data integration and Lorentz polarization, and so forth, corrections were made by the SMART software packages,[34] and numerical absorption corrections were applied using the X-RED/X-SHAPE program.[35] Full-matrix least-squares refinements on F_o^2 were performed with the aid of the SHELXTL v 6.1 program.[36]

Electronic Structure Calculations. Because of computing limitations, only the electronic structure of the 1/1 AC was calculated. The calculations were performed by means of the self-consistent, tight-binding, linear-muffin-tin-orbital (LMTO)[37−39] method in the local density (LDA) and atomic sphere (ASA) approximations, within the framework of the DFT method.[40] Interstitial spheres were introduced to achieve space filling. The ASA radii as well as the positions and radii of these empty spheres were calculated automatically. Reciprocal space integrations were carried out using the tetrahedron method. Down-folding techniques for outer Ca 4p, Au 5f, and Ga 4d orbitals were applied, and relativistic scalar effects were included in calculations. The band structure was sampled for 24 × 24 × 24 *k* points in the irreducible wedge of the Brillouin zone.

Results and Discussions

Syntheses and Phase Widths. The experience gained from earlier synthetic explorations[21,26,29] suggests that stoichiometric reactions of AB_xC_{6-x} (A, electropositive metal; B and C, electronegative metals) with $e/a = 2.0 \pm \sim 0.3$, are a good rule-of-thumb guide for possible Tsai-type AC/QC phases. In this study, the first exploratory synthesis of the target "$CaAu_4Ga_2$" yielded an essentially pure 2/1 AC phase according to its X-ray powder pattern. Later single-crystal structure analyses revealed a space group $Pa\bar{3}$, $a =$ 23.9377(8) Å, and a refined composition $Ca_{13}Au_{57.1(2)}Ga_{23.4(4)}$ ($e/a = 1.64$) or normalized, $Ca_{13.9}Au_{61.1(2)}Ga_{25.0(4)}$. The latter is consistent with the EDX result within 2σ, $Ca_{12.7(7)}Au_{62.1(9)}Ga_{25.2(1.4)}$. This result was very stimulating because it not only suggests that, according to experience, the corresponding 1/1 AC and i-QC phases both exist in this system, as confirmed by later synthetic results (Figure 1), but also reveals a 2/1 AC with an unexpectedly low *e/a* value. The *e/a* values for earlier Tsai-type 2/1 ACs are close to 2.0 or above, for example, 2.0 for $Ca_{13}Cd_{76}$,[41] 2.13 for $Sc_{11.2}Mg_{3.0}Zn_{73.5}$,[28] and 2.01 for $Ca_{12.6}Au_{37.0}In_{39.6}$.[29] Such a low *e/a* value suggests a similarly low value for the corresponding i-QC, too (1.84, observed) (below).

Figure 2 shows a portion of the phase distributions in the Ca−Au−Ga ternary system at 500 °C, in which differently colored pies key the product distributions among diverse compositions. (The i-QC is not stable at this temperature.) According to this work, four more unidentified phases exist in this system, and the earlier reported $Ca_3Au_{6.61}Ga_{3.39}$[42] and $CaAu_{0.5}Ga_{3.5}$[43] phases both occur within a single solid solution region. Two messages are new and of particular interest. First, compared with the Ca−Au−In system (Figure 2a in ref 29), the regions for 1/1 and 2/1 ACs here are roughly interchanged. This occurs because the present 2/1 AC is stable with higher percentages of gold in nearly all polya-

(32) Roisnel, T.; Rodríguez-Carvajal, J. *WinPLOTR: a Windows tool for powder diffraction patterns analysis*; 2000.
(33) Holland, T. J. B.; Redfer, S. A. T. *Miner. Mag.* **1997**, *61*, 65.
(34) *SHELXTL*; Bruker AXS, Inc: Madison, WI, 1997.
(35) *X-Shape, Program for numeric absorption*, version 1.03; Stoe & Cie: Darmstadt, Germany, 1998.
(36) *SHELXTL*; Bruker AXS, Inc: Madison, WI, 2000.
(37) Shriver, H. L. *The LMTO Method*; Springer-Verlag: Berlin, Germany, 1984.
(38) Anderson, O. K.; Jepsen, O. *Phys. Rev. Lett.* **1984**, *53*, 2571.
(39) Jepsen, O.; Snob, M. *Linearized Band Structure Methods in Electronic Band-Structure and its Applications*, Springer Lecture Note; Springer Verlag: Berlin, Germany, 1987.
(40) Tank, R.; Jepsen, O.; Burckhardt, A.; Andersen, O. K. *TB.LMTO-ASA Program*, Vers. 4.7; Max-Planck-Institut für Festkörperforschung: Stuttgart, Germany, 1988.
(41) Pay Gómez, C.; Lidin, S. *Angew.Chem., Int. Ed.* **2001**, *40*, 4037.
(42) Cordier, R.; Roehr, C.; Kussmann, D.; Hoffmann, R. D.; Poettgen, R. *Z. Anorg. Allg. Chem.* **2001**, *627*, 2053.
(43) Grin', Y.; Ellner, M.; Predel, B.; Cordier, G. *J. Alloys Compd.* **1994**, *216*, 207.

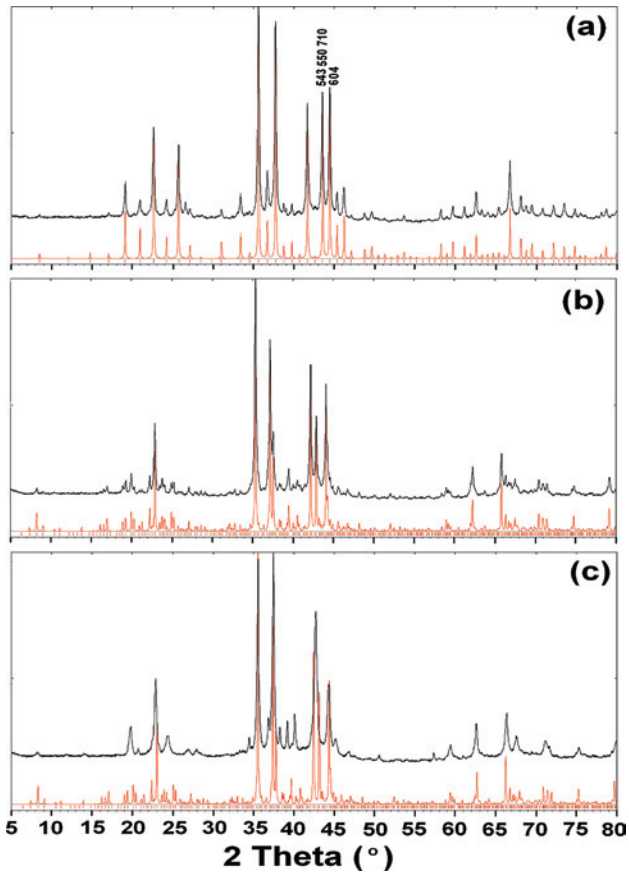

Figure 1. Experimental (black) and calculated (red) patterns according to single crystal refinement for (a) $Ca_3Au_{9.3}Ga_{9.7}$ 1/1 AC and (b) $Ca_{13}Au_{57.1}Ga_{23.4}$ 2/1 AC. In panel c, the calculated pattern of 2/1 AC is compared with the experimental pattern of the $Ca_{15.2}Au_{50.3}Ga_{34.5}$ i-QC. Small vertical red bars at the bottom of each panel mark the calculated peak positions.

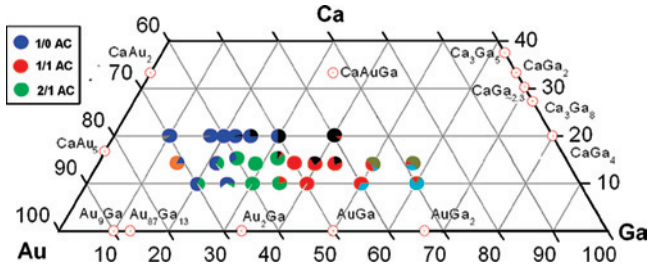

Figure 2. Portion of the phase distribution results for Ca−Au−Ga samples that were slowly cooled from 850 °C and annealed at 500 °C for three weeks. Inset codes are given for the AC and other phases. Dark gray, black, and olive colors key the known $CaAu_5$, $Ca_3(Au,Ga)_{11}$, and $Ca(Au,Ga)_4$, respectively. However, the last two exist as single solid solutions rather than as separate compositions. Orange, white, light gray, and cyan colors key the four unidentified phases, cf. Table 1.

nionic shells and thus has a smaller *e/a* value than the 1/1 AC (or the indium 2/1; Table 5). Second, a new phase type, a 1/0 AC $CaAu_{3+x}Ga_{1-x}$ ($x = 0-0.13$, $e/a = \sim 1.55-1.60$),[30] also appears in the present system, in contrast to the unrelated $Ca_4Au_{10}In_3$[44] near this region in the Ca−Au−In system. Obviously, electronic factors are not apt to be major factors in these changes because gallium and indium have same number of formal valence electrons; rather, size factors must have pronounced influences here, as expected. The DOS results are also very similar (below).

According to powder X-ray diffraction data, the lattice parameters for the 1/1 AC, Table 1, fall in the range of 14.6732(7)−14.790(1) Å, and for the 2/1 AC, 23.8829(9)−23.9816 (9) Å. These suggest considerable phase widths for both ACs at 500 °C, and single crystal results for three 1/1 AC samples obtained from different starting proportions confirm its large Au/Ga variation, that is, (9.2−12.1): (9.8−6.9). Moreover, these 1/1 AC samples are not at the phase boundaries (Figure 2), suggesting that a still larger composition ranges exist. For the 2/1 AC, Au/Ga variations are also expected, but only the structure of a crystal from the highest yield reaction is reported here since no new and interesting points seemed likely to be forthcoming.

A high yield (~80%) of i-QC phase (Figure 1c) was obtained via rapid quenching of nominal $CaAu_3Ga_3$ (*e/a* = 2.0) melt from 850 °C into cold water. (*Act quickly! The products are dominated by the 1/1 AC if the transfer from furnace into water and crushing of the SiO_2 container is delayed by several seconds.*) The quasilattice constant of this i-QC (refined by Elser's method[45] from the four strongest reflections within $2\theta = 35-45°$) is 5.350(2) Å. Note the relative peak positions between the four strongest peaks of the i-QC and the five strongest peaks of 1/1 and 2/1 ACs in Figure 1 and in the insets in Figure 3. These are the signature of the i-QC! The EDX composition of i-QC single crystals is $Ca_{15.2(5)}Au_{50.3(6)}Ga_{34.5(4)}$ (*e/a* = 1.84), close to two refined 1/1 ACs (*e/a* = 1.85 for crystal **2**, 1.76 for **3**) and 2/1 AC (1.64); see Table 1 and Figure 2. However, quenching of a nominal $CaAu_4Ga_2$ composition (*e/a* = 1.72) from 850 °C, which gives highest yield of 2/1 AC in a slow cooling and annealing process at 500 °C, yields a mixture of i-QC (~25%), $CaAu_3Ga$ 1/0 AC (~60%), and an unidentified phase (~15%). The quasilattice constant of this i-QC sample, 5.381(9) Å, is about 3.5σ larger than that obtained (~80% yield) from a nominal $CaAu_3Ga_3$ (*e/a* = 2.00) reaction. These results suggest that (1) the homogeneity range of the i-QC near 850 °C is smaller than that of corresponding 1/1 and 2/1 ACs at 500 °C (Table 1), and (2) the phase relationships are complex. Attempts to produce the i-QC from the suitable $CaAu_3Ga_3$ with the melt spinning method,[46] centrifuging at 660 °C to prevent phase change from i-QC to 2/1 AC (Figure 3b), gave only the 1/1 AC, probably because of the subsequent slow cooling. No further attempt was made to obtain pure i-QC.

Phase Stabilities. Figure 3 shows DTA data for the 1/1 AC (crystal **1**), the 2/1 AC (**4**), and the i-QC, respectively, together with insets of the powder patterns measured before and after DTA scans. Similar to the thermal behaviors of the Ca−Au−In 1/1 and 2/1 ACs,[29] both of the present 1/1 and 2/1 ACs are thermodynamically stable phases as they reform after the melting and solidification cycles, as shown by panels *a* and *b*. Although the Ca−Au−In 2/1 AC shows small peaks at ~502 °C in both heating and cooling data in

(44) Lin, Q.; Corbett, J. D. *Inorg. Chem.* **2007**, *46*, 8722.

(45) Elser, V. *Phys. Rev. B* **1985**, *32*, 4892.

(46) Fisher, I. R.; Islam, Z.; Panchula, A. F.; Cheon, K. O.; Kramer, M. J.; Canfield, P. C.; Goldman, A. I. *Philos. Mag. B.* **1998**, *77*, 1601.

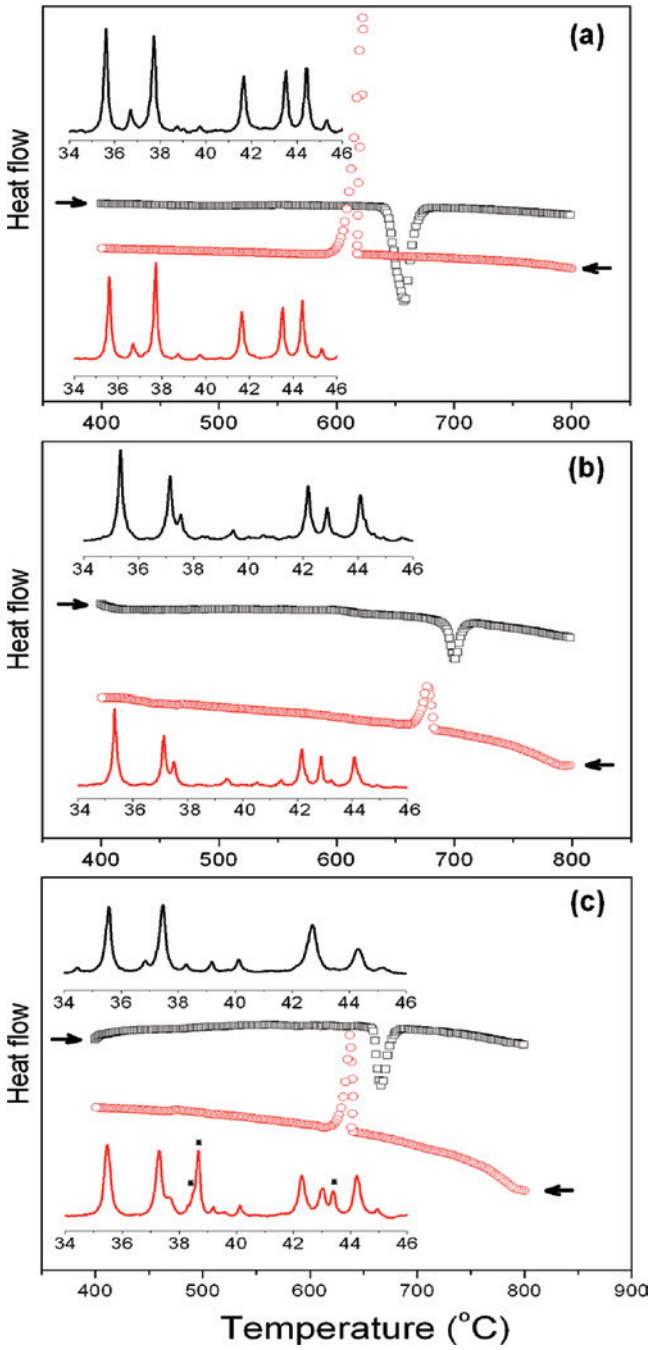

Figure 3. DTA data for (a) $Ca_3Au_{9.3}Ga_{9.7}$, 1/1 AC; (b) $Ca_{13}Au_{57.1}Ga_{23.4}$, 2/1 AC; and (c) $Ca_{15.2(5)}Au_{50.3(6)}Ga_{34.5(4)}$, i-QC. Black squares are DTA data on heating, and red circles, on cooling. Endothermic effects deflect downward. Black and red curves show the enlarged portion of X-ray patterns before and after each DTA scan. Peaks marked with stars in panel (c) are from the $Ca_3(Au,Ga)_{11}$ phase.

accord with $AuIn_2$ found in the powder pattern,[29] similar peaks do not appear in either pattern for the present 2/1 AC. The difference suggests that the present 2/1 AC melts congruently or nearly so at 692 °C.

At first glance, the thermogram cycle for the i-QC, Figure 3c, would suggest a stable i-QC phase because it shows only the melting/freezing processes at 659 ° and 638 °C, the difference originating with supercooling of the liquid. However, the powder X-ray diffraction patterns (inset) before and after reveal that a phase change occurs during the heating and cooling cycle, that is, the i-QC (plus ∼20% of an unidentified phase) transforms to ∼60% 2/1 AC and ∼40% $Ca_3(Au,Ga)_{11}$, a solid solution with structure of $Ca_3Au_{6.61}Ga_{4.39}$.[42] These processes exhibit ΔH values of −45.8 and −48.9 J/g, respectively, in the prescribed system according to the thermal analyses, the difference indicating that the Ca−Au−Ga i-QC phase is metastable at these and lower temperatures. This is of course in accord with the necessary synthetic conditions (quenching rather than slow cooling, during which the i-QC nucleates first; see Experimental Section). The spontaneous transition of i-QC to the primitive cubic 2/1 AC has only a small driving force, about −3.0 J/g in this system, and the complexity of the QC may also add some kinetic inhibition. In any case, no exotherm is observed on heating (at least at this heating rate, 10 °/min). Slow cooling instead results in the separation of the thermodynamically more stable 2/1 AC with the opposite and slightly greater enthalpy change. This seems to show a distinct parallel with the characteristics of the i-QC-1/1 AC conversion in the Li−Cu−Al system.[47] A more complex result is found on thermal analysis of the corresponding changes in the Ca−Au−In QC system,[29] which could be understood in terms of the re-separation of the QC closely followed by a similar exothermic effect at about 500 °C that was assigned to its decomposition to the 2/1 AC.

Structure Refinements. Assignments of space groups were made on the basis of the Laue symmetry and systematic extinction analyses. We note that all Ca−Au−Ga 1/1 AC single crystals checked exhibited 2 × 2 × 2 superlattice reflections in some CCD frames (not shown). However, superstructure refinements were not successful because the number of the observable superlattice reflections was small and the intensities, very low. Not surprisingly, all powder patterns reflections with $I/I_{max} > 0.05$ correspond to the basic unit cell, Figure 1a, even in the enlarged one (Figure 3a). Diffraction data from a higher energy source (e.g., a synchrotron) could yield the superstructure solution, but the sizable cost (of endeavor) for this analysis appears to be more than would be gained. Such a superstructure might be related to that of Eu_4Cd_{25},[48] the 2 × 2 × 2 superstructure of $EuCd_6$[49] which is also isostructural with YCd_6.[50]

Three 1/1 AC compositions were refined with the basic unit cell. The major influences of a superstructure on the average structure solution possibly would lie in the split positions, atom occupancies, and the displacement parameters. In these cases, the average U_{eq} values for all three 1/1 ACs are about 2−3 times larger than those for the 2/1 AC, and more split positions are found in the former too (below). All structural models were initialized by the direct methods, and some lower intensity positions, that is, those partially occupied or split, were later gained from the difference Fourier maps. As a check for correct compositions and site assignments, the occupancy parameters were

(47) Shen, Y.; Shiflet, G. L.; Poon, S. J. *Phys. Rev. B* **1988**, *38*, 5332.
(48) PayGómez, C.; Lidin, S. *Chem.—Eur. J.* **2004**, *10*, 3279.
(49) Pay Gómez, C.; Lidin, S. *Phys. Rev. B* **2003**, *68*, 024203.
(50) Villars, P.; Calvert, L. D. *Pearson's Handbook of Crystallographic Data for Intermetallic Phases*, 2nd ed.; American Society of Metals: Materials Park, OH, 1991; Vol. *1*.

Table 2. Some Data Collection and Refinement Parameters for Three 1/1 (**1**, **2**, **3**) and a 2/1 (**4**) ACs in the Ca−Au−Ga system

	1/1 AC			2/1 AC
	1	**2**	**3**	**4**
refined comp.	$Ca_3Au_{9.3(1)}Ga_{9.7(2)}$	$Ca_3Au_{11.1(1)}Ga_{7.9(1)}$	$Ca_3Au_{12.1(1)}Ga_{6.9(1)}$	$Ca_{13}Au_{57.1(2)}Ga_{23.4(4)}$
normalized comp.	$Ca_{13.6}Au_{42.3(4)}Ga_{44.1(8)}$	$Ca_{13.6}Au_{50.5(4)}Ga_{35.9(4)}$	$Ca_{13.6}Au_{55.0(4)}Ga_{31.4(4)}$	$Ca_{13.9}Au_{61.1(2)}Ga_{25.0(4)}$
e/a	2.02	1.85	1.76	1.64
f.w.	2624.5	2853.1	2981.4	13401.5
space group/*Z*	$Im\bar{3}/8$	$Im\bar{3}/8$	$Im\bar{3}/8$	$Pa\bar{3}/8$
latt. const. (Å)	14.6941(6)	14.7306(6)	14.7594(6)	23.9377(8)
V (Å^3)/d_{cal} (Mg/m^3)	3172.7(2)/10.99	3196.4(2)/11.86	3215.2(2)/12.32	13716.6(8)/12.98
refl. coll./R_{int}	10017/0.0874	10142/0.0763	10195/0.0780	83761/0.2518
indep.refl./restr./para.	720/0/54	730/0/59	740/0/64	5622/0/333
GOF on F^2	1.089	1.035	1.091	1.052
R1/wR2 [$I > 2\sigma(I)$][a]	0.0581/0.1400	0.0453/0.1105	0.0443/0.1118	0.0520/0.0977
[all data]	0.0774/0.1488	0.0642/0.1180	0.0505/0.1153	0.1333/0.1102

[a] $R1 = \sum||F_o| - |F_c||/\sum|F_o|$; $wR2 = \{[\sum[w(F_o^2 - F_c^2)^2]/\sum[w(F_o^2)^2]\}^{1/2}$.

Table 3. Atomic Coordinates and Isotropic Equivalent Displacement Parameters for Ca−Au−Ga 1/1 ACs (crystals **1**, **2**, and **3**)[a]

atom	Wyck.	symm.	occ. (%)	*x*	*y*	*z*	U_{eq}(Å^2)
			$Ca_3Au_{9.3(1)}$ $Ga_{9.8(2)}$(1)				
Au1	24*g*	*m*..		0	0.4013(1)	0.3545(1)	0.058(1)
Au/Ga2	48*h*	1	47.2/52.8(8)	0.1071(1)	0.3412(1)	0.1985(1)	0.051(1)
Ga3	12*e*	*mm*2..		0.2039(3)	0	1/2	0.060(2)
Au4	16*f*	.3.	77.2(6)	0.1528(1)	*x*	*x*	0.045(1)
Ga4	16*f*	.3.	22.8(6)	0.1079(8)	*x*	*x*	0.045(1)
Au5	24*g*	*m*..	50(1)	0	0.2524(3)	0.0870(4)	0.042(1)
Ga5	24*g*	*m*..	50(1)	0	0.2239(9)	0.086(1)	0.042(1)
Ga6	12*d*	*mm*2..		0.4101(4)	0	0	0.070(2)
Ga7	24*g*	*m*..	33.3	0	0.061(1)	0.0829(8)	0.066(4)
Au/Ga8	8*c*	.−3.	38/62(3)	1/4	1/4	1/4	0.31(2)
Ca	24*g*	*m*..		0	0.1870(4)	0.3025(4)	0.038(1)
			$Ca_3Au_{11.1(1)}Ga_{7.9(1)}$ (2)				
Au1	24*g*	*m*..		0	0.4031(1)	0.3546(1)	0.037(1)
Au/Ga2	48*h*	1	75.1/24.9(6)	0.1044(1)	0.3408(1)	0.1972(1)	0.040(1)
Ga3	12*e*	*mm*2..		0	1/2	0.2001(3)	0.040(1)
Au4	16*f*	.3.		0.1506(1)	*x*	*x*	0.031(1)
Ga5	24*g*	*m*..	75.6(4)	0	0.2660(4)	0.0817(4)	0.021(1)
Au5	24*g*	*m*..	24.4(4)	0	0.2265(4)	0.0908(4)	0.021(1)
Au/Ga6	12*d*	*mm*2..	40/60(1)	−0.1006(3)	1/2	1/2	0.058(1)
Ga7	24*g*	*m*..	25(2)	0.091(2)	0.084(1)	0	0.039(3)
Au7	24*g*	*m*..	7.7(9)	0.036(2)	0.081(1)	0	0.022(4)
Ga8	8*c*	.−3.		1/4	1/4	1/4	0.079(3)
Ca	24*g*	*m*..		0	0.1884(3)	0.3049(3)	0.025(1)
			$Ca_3Au_{12.1(1)}Ga_{6.9(1)}$ (3)				
Au1	24*g*	*m*..		0	0.3564(1)	0.4036(1)	0.034(1)
Au/Ga2	48*h*	1	87.4/12.6(7)	0.1033(1)	0.1990(1)	0.3405(1)	0.039(1)
Ga3	12*e*	*mm*2..		0	1/2	0.2995(2)	0.035(1)
Au4	16*f*	.3.		0.1497(1)	*x*	*x*	0.031(1)
Au5	24*g*	*m*..	27.4(8)	0.2678(5)	0	0.0777(3)	0.033(1)
Ga5	24*g*	*m*..	72.6(8)	0.2278(6)	0	0.0903(3)	0.031(1)
Ga6	12*d*	*mm*2..	48.2(8)	−0.1109(3)	1/2	1/2	0.037(1)
Au6	12*d*	*mm*2..	51.8(8)	−0.0714(9)	1/2	1/2	0.037(1)
Ga7	24*g*	*m*..	9.3(6)	0.0848(7)	0.093(1)	0	0.036(4)
Au7	24*g*	*m*..	24.0(6)	0.0784(7)	0.040(1)	0	0.029(2)
Ga8	8*c*	.−3.		1/4	1/4	1/4	0.059(2)
Ca	24*g*	*m*..		0	0.3061(3)	0.1885(3)	0.029(1)

[a] $U_{eq} = (U_{11} + U_{22} + U_{33})/3$.

refined in a separate series of refinements, along with isotropic displacement parameters. All sites with standard deviations within 3σ of unity are considered to be fully occupied in the final least-squares refinements with anisotropic displacement parameters.

Some data collection and crystallographic data, and structure refinement parameters are given in Table 2, and other relevant and more detailed information is listed in Table S1 in Supporting Information. The refined positional and isotropic-equivalent displacement parameters for the 1/1 ACs are listed in Table 3, and for the 2/1, in Table 4. Note that the 2/1 AC exhibits the characteristically larger number of relatively weak reflection data, resulting in the generally larger R_{int} and R1 values for all data (Table 2).

Remarkably, in all three Ca−Au−Ga 1/1 AC samples at our level of refinement, atoms at the cube centers and in the innermost tetrahedra (below) have full and one-third occupancies (within 3σ), respectively. This leads to a ratio of 3:19 between electropositive and negative elements, thus representing stoichiometric derivatives of the YCd_6 prototype.[20] In addition, Au/Ga8 in crystal **1** exhibits very large displacement parameters, regardless of whether a Au/Ga

Table 4. Atomic Coordinates and Isotropic Equivalent Displacement Parameters for crystal **4**, the $Ca_{13}Au_{57.1(2)}Ga_{23.4(4)}$ 2/1 AC[a]

atom	Wyck.	symm.	occ. (%)	*x*	*y*	*z*	U_{eq} (Å^2)
Au1	24*d*	1		0.0953(1)	0.1559(1)	0.2524(1)	0.015(1)
Au2	24*d*	1		0.0982(1)	0.1561(1)	0.4465(1)	0.015(1)
Au3	24*d*	1		0.2171(1)	0.1548(1)	0.2555(1)	0.019(1)
Au4	24*d*	1		0.2176(1)	0.1500(1)	0.4395(1)	0.020(1)
Au5	24*d*	1		0.0405(1)	0.2542(1)	0.4108(1)	0.018(1)
Au6	24*d*	1		0.2875(1)	0.1982(1)	0.3459(1)	0.019(1)
Au7	24*d*	1		0.0573(1)	0.0969(1)	0.1567(1)	0.024(1)
Au8	8*c*	.3.		0.0620(1)	*x*	*x*	0.016(1)
Au9	24*d*	1		0.0416(1)	0.2566(1)	0.2874(1)	0.019(1)
Au10	24*d*	1		−0.029(1)	0.3454(1)	0.2103(1)	0.018(1)
Au11	24*d*	1		0.0360(1)	0.0571(1)	0.4127(1)	0.017(1)
Au12	24*d*	1		0.0922(1)	0.3464(1)	0.3545(1)	0.028(1)
Au13	24*d*	1		0.0362(1)	0.4432(1)	0.4050(1)	0.026(1)
Au14	24*d*	1		0.1363(1)	0.0964(1)	0.3488(1)	0.022(1)
Au15	24*d*	1	37.2(6)	−0.1026(5)	0.3669(4)	0.1570(8)	0.21(1)
Au/Ga16	24*d*	1	88.7/11.3(9)	0.2847(1)	0.0464(1)	0.4337(1)	0.026(1)
Au/Ga17	24*d*	1	94/6(1)	−0.0654(1)	0.4437(1)	0.2438(1)	0.032(1)
Au/Ga18	24*d*	1	69.3/30.7(9)	0.0334(1)	0.0524(1)	0.2754(1)	0.033(1)
Au/Ga19	24*d*	1	60.4/39.6(9)	−0.0249(1)	0.1484(1)	0.2390(1)	0.031(1)
Au/Ga20	24*d*	1	45/55(1)	−0.0638(1)	0.2525(1)	0.2393(1)	0.038(1)
Au21	24*d*	1	75.4(8)	−0.0908(1)	0.1969(1)	0.1581(1)	0.040(1)
Ga21	24*d*	1	24.6(8)	−0.0632(8)	0.1646(8)	0.1522(8)	0.027(4)
Au22	24*d*	1	46(1)	−0.0350(2)	0.1341(2)	0.0918(4)	0.041(2)
GA22	24*d*	1	54(1)	−0.0209(2)	0.1524(3)	0.0607(3)	0.043(2)
Ga23	8*c*	.3.		0.1563(1)	*x*	*x*	0.012(1)
Ga24	24*d*	1		0.1579(2)	0.1509(2)	0.5395(1)	0.016(1)
Ga25	4*b*	.−3.		0	0	1/2	0.024(2)
Ga26	24*d*	1		−0.0992(2)	0.4883(2)	0.1553(2)	0.038(1)
Ga27	24*d*	1		0.2443(2)	0.0995(2)	0.3433(2)	0.035(1)
Ga28	8*c*	.3.		0.2659(2)	*x*	*x*	0.026(2)
Ga29	24*d*	1		−0.1211(3)	0.3494(3)	0.2132(3)	0.063(2)
Ga30	24*d*	1	64(2)	0.0393(3)	0.3476(3)	0.4617(2)	0.023(2)
Ga31	24*d*	1	33(2)	0.0950(5)	0.3557(7)	0.4534(5)	0.034(5)
Ga32	24*d*	1	33(2)	0.060(6)	0.3177(6)	0.5091(6)	0.030(5)
Ca1	8*c*	.3.		−0.0407(3)	*x*	*x*	0.018(3)
Ca2	24*d*	1		0.3479(3)	0.1582(3)	0.4620(3)	0.014(1)
Ca3	24*d*	1		−0.1528(3)	0.1574(3)	0.2705(3)	0.013(1)
Ca4	24*d*	1		0.0388(3)	0.2303(3)	0.1561(3)	0.012(1)
Ca5	24*d*	1		0.1548(3)	0.0335(3)	0.4639(3)	0.011(1)

[a] $U_{eq} = (U_{11} + U_{22} + U_{33})/3$.

Table 5. Comparison of Shell Contents within Triacontahedra in the Ca−Au−Ga and Ca−Au−In ACs

	Ca−Au−Ga		Ca−Au−In	
	1/1[a]	2/1	1/1	2/1
formula	$Ca_3Au_{12.1(1)}Ga_{6.9(1)}$	$Ca_{13}Au_{57.1(2)}Ga_{23.4(4)}$	$Ca_3Au_{12.2(1)}In_{6.3(2)}$	$Ca_{12.6(1)}Au_{37.0(2)}In_{39.6(6)}$
(*e*/*a*)	(1.76)	(1.64)	(1.74)	(2.01)
tetrahedron[b]	$Au_{2.8}Ga_{1.2}$	$Au_{1.2}Ga_3$	In_4	$In_{3.5}$
dodecahedron	$Au_{11.3}Ga_{8.7}$	$Au_{13.3}Ga_{6.7}$	$Au_{15.3}In_{4.7}$	$Au_{10.2}In_{9.3}$
icosahedron	Ca_{12}	Ca_{12}	Ca_{12}	Ca_{12}
icosidodecahedron	$Au_{23.9}Ga_{6.1}[Ga_8]$[c]	$Au_{26.1}Ga_{3.9}[Ga_9]$[c]	$Au_{20.7}In_{9.3}[In_{3.8}]$[c]	$Au_{11.0}In_{19.0}[In_{1.6}]$[c]
triacontahedron	$Au_8Ga_{24}(Au_{56.9}Ga_{3.1})$[d]	$Au_7Ga_{21.9}(Au_{57.3}Ga_{2.7})$[d]	$Au_{6.8}In_{25.2}(Au_{54.0}In_{6.0})$[d]	$In_{29.6}(Au_{48.0}In_{12.0})$[d]
Reference	this work	this work	29	29

[a] The data for the 1/1 AC are from crystal **3**. [b] Disordered tetrahedron in 1/1 and fractional tetrahedron in 2/1 AC. [c] Contents in square brackets are fractional atoms located between shells. [d] Contents in parentheses are additional decorations at or near the center of the edges of the triacontahedral clusters.

admixture or partial occupancy of Au [62(2) %] is refined in this position. Such a result is, however, consistent with the observed electron density map, as shown in Figure 4f. Apparently, the displacement parameters relate to the synthetic conditions: crystal **2** and **3**, which were annealed, exhibit much smaller U_{eq} values (0.079 and 0.059 Å^2, respectively) than does crystal **1**, which came from a sample centrifuged at 660 °C and not annealed [0.31(2) Å^2]. The observed electron densities about the tetrahedra in crystal **2** and **3** are also somewhat different from those in crystal **1**. The former are peanut-shaped (not shown), suggesting split atoms at these positions, whereas the contrasting electron densities for the nominal tetrahedron in crystal **1** are in more diffuse and crenel-shaped (Figure 1g).

Crystal Structures. As before,[28,29,49] the 1/1 AC structure consists of body-centered-cubic packing of interpenetrating triacontahedral clusters, within which the so-called Tsai cluster sequence[19] is encapsulated. The latter refer to an assembly of four endohedral shells, from the center out, a disordered tetrahedron, a pentagonal dodecahedron, an icosahedron, and an icosidodecahedron, as shown in Figure 4a−d. From another viewpoint,[41,51] each triacontahedral cluster also contains eight cubes on the 3-fold axes, as shown in Figure

(51) Piao, S.; Gomez, C. P.; Lidin, S. *Z. Naturforsch.* **2006**, *61B*, 644.

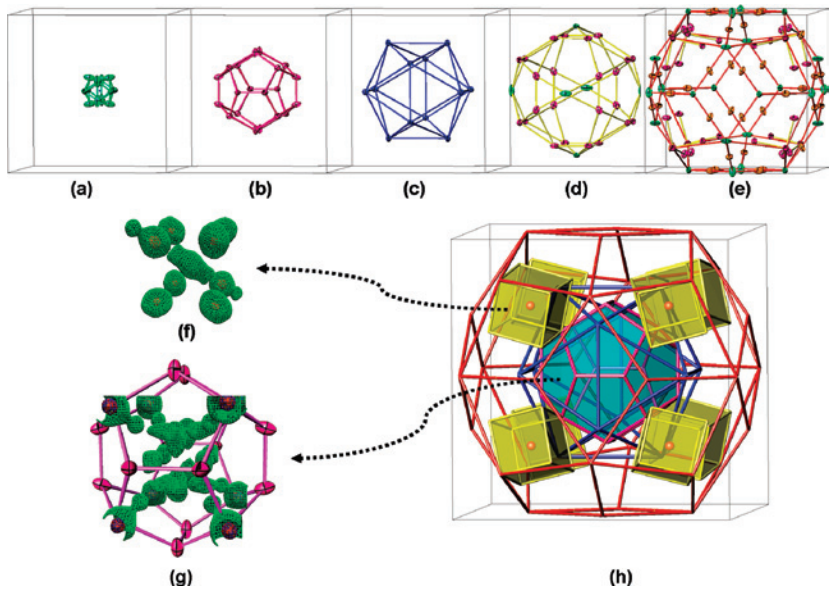

Figure 4. Each triacontahedral cluster in Ca−Au−Ga 1/1 AC contains five shells, namely, (a) a 3-fold disorder tetrahedron, (b) a pentagonal dodecahedron, (c) an icosahedron of Ca, (d) an icosidodecahedron, and (e) a triacontahedron. The last shell also contains 60 decoration atoms, which are located nearby the midedges; (f) and (g) show the observed electron densities about the cube and tetrahedron in crystal **1**. The cutoff contour level is 8.0 e/Å^3. (h) Cubes within a triacontahedral cluster. The cube center corresponds to the Wyckoff 8 *c* position in the 1/1 ACs. Like cubes with distortions also exist in 2/1 AC. Au is represented gold spheres, Ga by cyan, Ca by blue, and Au/Ga mixtures by purple. The same holds for Figure 5.

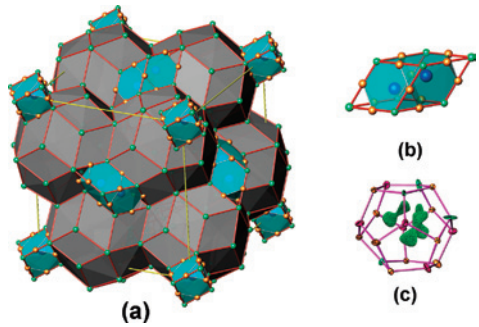

Figure 5. (a) Polyhedral view of the unit cell of $Ca_{13}Au_{57.1}Ga_{23.4}$ 2/1 AC, featuring simple cubic packing ($Pa\bar{3}$) of triacontahedral clusters (dark gray) and prolate rhombohedra (cyan). Some atoms near the midedges in (a) are omitted for clarity; one of the latter is shown in (b). The triacontahedral cluster also contains five shells, but the innermost tetrahedron has a monotruncated tetrahedral geometry, as shown in the observed electron density map in (c). The cutoff contour level in (c) is 8.0 e/Å^3.

4h. Each cube consists of a 3-fold vertex of the dodecahedron, three vertices (forming a triangle face) of the icosidodecahedron, and a 3-fold vertex and three midedge atoms of the outmost triacontahedron. Such cubes can have profound influences on phase widths and stability because the cube centers can be partially occupied or empty, and this allows certain variations in composition and *e/a*. For example, the cubes are empty at $y < \sim 2.0$ and have 24% Zn at $y = 2.2$ in the $Sc_3Cu_yZn_{18-y}$ series,[21] and are about half-occupied by indium in $Ca_3Au_{12.2}In_{6.3}$ 1/1 AC.[29] In the present 1/1 ACs, the cube centers are, evidently for the first time, found to be fully occupied (Table 3).

Lidin and co-workers[49,51] have noted that the cubes, the dodecahedra, and the innermost disordered tetrahedra in $RCd_{6+\delta}$ (R = rare earth metal) are actually intercorrelated. That is, occupation of the cube centers is accompanied by a deformation of the dodecahedral shell and a partial orientational ordering of the innermost tetrahedra. The same holds for the Ca−Au−Ga 1/1 ACs, except that the dodecahedral cage deforms to give apparent split positions (disorder) rather than via an extrusion or shrinkage of the cage. The reason might be related to size mismatching between Au and Ga and the existence of a superstructure.

The $Ca_{13}Au_{57.1(2)}Ga_{23.4(4)}$ 2/1 AC, Figure 5a, contains simple cubic packing of triacontahedral and prolate rhombohedral clusters (a prolate rhombohedron is a cube elongated along a 3-fold axis, Figure 5b). The latter are interstitials in the former. The geometries for the five shells in the triacontahedra are similar to those in 1/1 AC, except that greater distortions in 2/1 are allowed by the lower symmetry. Because cluster linkages (long-range order) in the present 2/1 AC are similar to those reported earlier,[28,29] we will not reiterate the detailed structure descriptions here. The most pronounced difference is the geometry of the innermost so-called tetrahedra, Figure 5c, for which the observed electron densities more resemble a monotruncated rather than a regular tetrahedron. However, the refined content of this shell is still about four atoms.

Table 5 lists the comparative shell contents for the Ca−Au−Ga and Ca−Au−In 1/1 and 2/1 ACs. Direct comparison between 2/1 ACs shows that the gallium content in the former is less than the indium content in the latter for all corresponding shells except the third icosahedral shells. In addition, the present 1/1 and 2/1 ACs contain more interstitials between the icosidodecahedral and the triacontahedral shells than do the indides. These interstitial atoms are actually the centers of cubes in 1/1 (Figure 4g) and of distorted cubes in 2/1 AC. It is noteworthy that all of them are dominated by Ga, namely, Ga8 in the 1/1 ACs (except that this position in crystal **1** also contains ~32% Au), and Ga25, Ga27, Ga31, and Ga32 in the 2/1 AC. A size factor is evident here: on one hand, the cube center-to-vertex distances in the Ca−Au−In 1/1 AC (2.548−2.638Å) are too

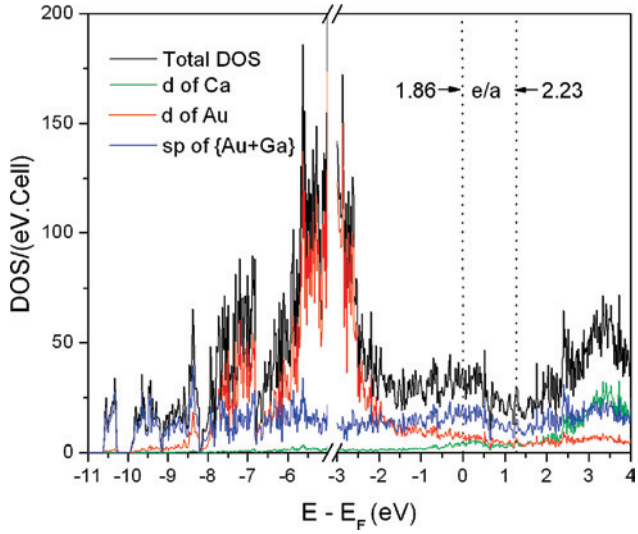

Figure 6. Total and projected partial densities-of-states (DOS) for a hypothetical disorder-free "$Ca_{24}Au_{88}Ga_{64}$" 1/1 AC, $e/a = 1.86$.

small to allow fully occupied In centers, but parallel distances in the present 1/1 ACs (2.473−2.656 Å) fall in the range of normal Au−Ga and Ga−Ga distances (Au, 1.339Å; In, 1.421 Å; Ga, 1.246 Å from Pauling's single metallic bonds[52]). On the other hand, distortions of the cubes in the 2/1 Ca−Au−Ga AC result in center-to-vertex distances that are too small; thus the centers can only be partially occupied.

Electronic structure of 1/1 AC. An LMTO-ASA calculation necessarily requires a disorder-free structural model; therefore, the disorder present in the 1/1 AC needs to be technically handled prior to the calculation. The following steps were applied: (1) each pair of split positions was represented by its average; (2) mixed positions were considered as fully occupied by the predominant component; and (3) the disordered tetrahedra were circumvented by reduction of the symmetry to *I*23 and a slight reorientation to match the symmetry requirements. Such treatments give negligible differences in total energies, as before.[26,28,53] These lead to a model (Table S2 in Supporting Information) with a unit cell content of "$Ca_{24}Au_{88}Ga_{66}$" ($e/a = 1.86$), which is close to that of crystal **2** ($e/a = 1.85$) and near the middle of the observed 1/1 AC composition range.

Figure 6 shows the DOS for this hypothetical defect-free "$Ca_{24}Au_{88}Ga_{64}$" 1/1 AC. In comparison, the pattern naturally exhibits close to the same projected DOS and scales as published for the Ca−Au−In 1/1 AC (Figure 7 in ref 29). As can be seen, the total DOS profile is very spiky, characteristic of ACs (because of high degeneracies). The Au d orbitals are populated mainly over ∼ −6.0 to −2.0 eV, whereas the s, p orbitals of Au and Ga are spread over the whole spectrum, and the Ca 3d falls around the Fermi energy (E_F) and above. Although the total Ca d contribution appears comparable to that of Au d over the energy range of 0−2.3 eV, the former's actual effect here is much greater because the total number of Ca per cell is only about a quarter of that of Au. The total DOS curve exhibits a shallow dip (pseudogap) centered at about ∼1.2 eV ($e/a \approx 2.23$), and its appreciable nonzero DOS at E_F suggests a metallic property. All these features are very similar to those in the Ca−Au−In 1/1 AC[29] except that the present pseudogap is not as deep as for its In neighbor.

Somewhat surprising is that e/a for the i-QC $Ca_{15.2(5)}Au_{50.3(6)}Ga_{34.5(4)}$, 1.84, falls near that for the 1/1 composition used for the calculation, 1.86, and appreciably below that of the calculated pseudogap, 2.23. However, this does not mean the Hume−Rothery mechanism is not operable in this system. According to the LMTO calculations, the diameter of the Fermi sphere ($2K_F$) is 1.56 Å, close to the center-to-surface distance ($K_p \approx 1.54$ Å) of the Brillouin zone constructed from {5 4 3}{7 1 0}{5 5 0} and {6 0 4} Miller planes of the 1/1 ACs according to $K_p = \pi(h^2 + k^2 + l^2)^{1/2}/a$.[13] These Miller planes generate two strong reflections at 43.52° and 44.42°, which encompass the diffraction peak of the i-QC at 44.31° (see panels a and c in Figure 1). This suggests that the spherical Fermi surface in the i-QC would touch the Brillouin zone constructed from Miller planes that are responsible for the diffraction peak at 44.31°. In other words, although the e/a value for the Ca−Au−Ga i-QC is not located in the calculated pseudogap, the phase still appears to follow the Hume−Rothery mechanism,[13] and the pseudogap prediction may be the weak point. In addition, the Hume−Rothery stabilization mechanism may not be the predominant factor in this QC system; on the contrary, the contribution of orbital mixing between the low-lying Ca d and the Au and Ga s, p is large around E_F and above for the model 1/1, as shown in Figure 6. The same situation is also calculated for the binary Cd-based 1/1 AC.[53]

Conclusions

Synthetic explorations to tune to Ca−Au−Ga ACs and i-QC phases have been carried out according to experiences that gallium and indium play similar roles in polar intermetallics. Thus, the structural differences between Ca−Au−In and Ca−Au−Ga ACs appear mainly as direct results of the size difference between In and Ga. These include the facts that (1) the cube centers in the present 1/1 AC structures are fully occupied by the smaller Ga, resulting in a 3:19 stoichiometric derivative of the YCd_6 prototype; (2) the present 2/1 AC has lower e/a value than the 1/1, in contrast to those for Ca−Au−In; (3) the e/a value for the Tsai-type i-QC is the first one as low as 1.84.

Acknowledgment. We thank Kevin W. Dennis for the permission to use the DTA instruments. This research was supported by the U.S. National Science Foundation, Solid State Chemistry, via Grant DMR-0444657 and was performed in facilities of the Ames Laboratory, U.S. Department of Energy, at Iowa State University.

Supporting Information Available: Tables S1−S2 and a CIF file for four crystal structures. This material is available free of charge via the Internet at http://pubs.acs.org.

IC800694J

(52) Pauling, L. *The Nature of the Chemical Bond*; 3rd ed.; Cornell University Press: Ithaca, 1960; p 403.
(53) Ishii, Y.; Fujiwara, T. *Phys. Rev. Lett.* **2001**, *87*, 206408.